Applied Physics Letters ARTICLE pubs.aip.org/aip/apl

Theoretical defect engineering in $AgBiI_4$ for enhanced photovoltaic performance

Cite as: Appl. Phys. Lett. **127**, 042101 (2025); doi: 10.1063/5.0275404
Submitted: 12 April 2025 · Accepted: 11 July 2025 ·
Published Online: 28 July 2025

Quanhe Yan,[1] Haoze Li,[1] Zhongyi Luo,[1] Haoyu Cao,[1] Rasha A. Awni,[2] Run Xu,[3,4] Weiwei Meng,[5,a)] Fei Xu,[1,4,a)] and Feng Hong[1,4,a)]

AFFILIATIONS

[1]SHU-Solar E R&D Lab, Shanghai Key Laboratory of High Temperature Superconductors, Department of Physics, College of Sciences, Shanghai University, Shanghai 200444, China
[2]Department of Electrical Engineering, College of Engineering, University of Baghdad, Baghdad 10071, Iraq
[3]Department of Electronic Information Materials, School of Materials Science and Engineering, Shanghai University, Shanghai 200444, China
[4]Zhejiang Institute of Advanced Materials, Shanghai University, Jiashan 314113, China
[5]South China Academy of Advanced Optoelectronics, South China Normal University, Guangzhou 510006, China

[a)]**Authors to whom correspondence should be addressed:** wwmeng@m.scnu.edu.cn; feixu@shu.edu.cn; and fenghong@shu.edu.cn

ABSTRACT

Silver-bismuth iodide (ABI) ternary semiconductors, such as $AgBi_2I_7$, $AgBiI_4$, Ag_2BiI_5, and Ag_3BiI_6, have emerged as promising lead-free light absorbers for photovoltaic applications due to their favorable optoelectronic properties. Despite recent advances that have improved power conversion efficiencies from ~1% to over 5%, ABI-based solar cells still show substantial open-circuit voltage (V_{OC}) losses of up to ~1 V, which significantly hinder the device performance. These losses have been experimentally attributed to the non-radiative recombination originating from intrinsic defects, however, theoretical understanding of these defect mechanisms remains limited. Here, using density functional theory calculations, we systematically investigate the defect properties of $AgBiI_4$. We identify the dominant intrinsic defects as acceptor-like Ag vacancies (V_{Ag}) and Ag_{Bi} antisites, as well as donor-like Ag interstitials (Ag_i) and Bi_{Ag} antisites. Among these defects, V_{Ag} and Ag_{Bi} are shallow defects, while Ag_i and Bi_{Ag} create deep trap states. Our calculations reveal that I-rich synthesis conditions with a carefully balanced Ag/Bi ratio are essential to suppressing the formation of deep defects and mitigating non-radiative recombinations. These insights provide theoretical guidance for defect modulation in ABI compounds and highlight $AgBiI_4$ as a model system for understanding defect physics in ABI photovoltaic materials.

Metal-halide octahedral inorganic framework semiconductors have demonstrated enormous potential for photovoltaic applications owing to their exceptional electronic and optical properties. Typically, metals with ns^2 (e.g., Pb and Sn in perovskites)[1] or nd^{10} (e.g., Cu and Ag in double perovskites)[2] electron configurations give rise to an occupied antibonding valence band maximum (VBM), enabling strong *d*/*p*-*p* transitions. These transitions support efficient light harvesting, high carrier mobility, and enhanced defect tolerance. Through the combination of Ag ($4d^{10}$) and Bi ($6s^2$), the $Ag_xBi_yI_{x+3y}$ (ABI) ternary compound has emerged as a promising candidate for lead-free photovoltaic light absorbers, offering low toxicity, excellent chemical stability, and a high optical absorption coefficient (~10^5–10^6 cm^{-1}).[3–5] Moreover, the diversity of elemental composition in ABI enables flexible tuning of material properties, thereby benefiting their photovoltaic and optoelectronic applications.[3,6–13]

The ABI system comprises a variety of compounds with different Ag/Bi atomic ratios, such as $AgBi_2I_7$,[10] $AgBiI_4$,[11] Ag_2BiI_5,[12] and Ag_3BiI_6.[13] All of these compounds retain edge-sharing octahedral units and have been reported to exhibit photovoltaic activity, thereby meeting the fundamental requirements for light absorbers in solar cells. Kim *et al.*[3] pioneered the work in 2016, initially exploring the potential of $AgBi_2I_7$ for photovoltaic applications and fabricating a solar cell with a power conversion efficiency (PCE) of 1.22%. Subsequently, a series of studies on the photovoltaic properties of various ABI compounds have reported that $AgBiI_4$-based,[6] Ag_2BiI_5-based,[7] and Ag_3BiI_6-based[8] cells initially achieved PCEs of 0.41%, 2.1%, and 4.3%,

respectively. Based on the advancements in synthetic procedures and an increase in the level of sulfide anionic substitution, Pai *et al.*[9] successfully prepared a series of compounds, improving the PCEs of $AgBi_2I_7$ to 2.48%, $AgBiI_4$ to 2.75%, Ag_2BiI_5 to 3.91%, and Ag_3BiI_6 to 5.56%. Although the PCEs of ABI-based solar cells have been improved, a substantial gap still exists compared to the 27% theoretical Shockley–Queisser limit efficiency associated with a typical bandgap of 1.8 eV of ABI.[14] ABI solar cells typically exhibit open circuit voltage (V_{OC}) ranging from 0.5 to 0.8 V,[3,6–9] which is significantly lower than the 1.5 V radiative limit for a 1.8 eV absorber.[15] Figure 1(a) demonstrates the PCEs and the corresponding V_{OC} deficits of ABI-based solar cells collected from the literature. The values in Fig. 1(a) are listed in Table S1. These solar cells experienced a considerable V_{OC} loss around 1 V. Initially, researchers attributed this large V_{OC} deficit to the non-radiative combination that is triggered by pinholes and shunt paths in the solution processed thin films with inferior quality. However, subsequent experiments have demonstrated that the PCE is still below 3% despite the improvements in ABI film quality.[4,16,17] For instance, Khazaee *et al.*[16] obtained pinhole-free $AgBi_2I_7$ films deposited by thermal evaporation with a PCE of 0.9%. Through dynamic hot casting, Ghosh *et al.*[4] have achieved pinhole-free Ag_2BiI_5 films with a PCE of 2.5%. Correa Guerrero *et al.*[17] optimized the content of BiI_3 to get opaque films of Ag_2BiI_5 with a PCE of 2%. This has led to the recognition that the non-radiative recombination originating from intrinsic defects is the primary cause of V_{OC} losses.[15] Subsequently, experimental research has been carried out to understand the defect properties of ABI materials. Merker *et al.*[18] observed evidence of a 0.6 eV defect level within the bandgap in $AgBi_2I_7$ through Fourier-transform step-scan photocurrent spectroscopy (FTPS). Pecunia *et al.*[19] reported two defect levels of 0.33 and 0.25 eV within the bandgap of $AgBiI_4$ using photocurrent transient spectroscopy (PICTS). These defects exhibited small capture cross sections of approximately 10^{-19} cm^2. Thus, they proposed that $AgBiI_4$ has acceptable defect tolerance. Bera *et al.*[20] employed Kelvin probe force microscopy (KPFM) and scanning tunneling spectroscopy (STS) to investigate the composition-dependent Fermi energy tuning and *p*- to

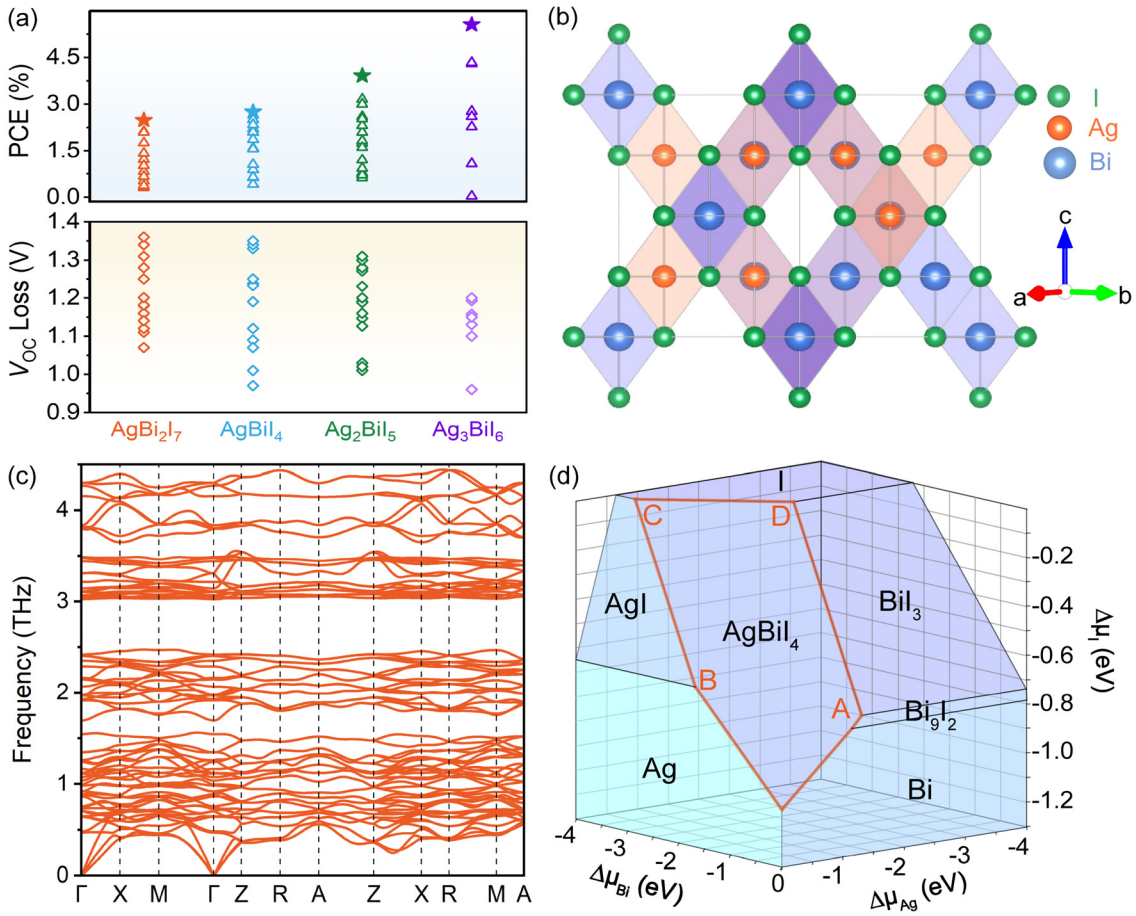

FIG. 1. (a) PCEs and the corresponding V_{OC} losses of ABI-based solar cells collected from the literature. (b) Crystal structure of $AgBiI_4$. The tangerine, blue, and green spheres represent Ag, Bi, and I atoms. (c) Phonon spectrum and (d) phase diagram of $AgBiI_4$. Four representative chemical potential points in (d): point A ($\Delta\mu_{Ag} = -1.32$ eV, $\Delta\mu_{Bi} = 0$ eV, $\Delta\mu_I = -0.74$ eV); B ($\Delta\mu_{Ag} = 0$ eV, $\Delta\mu_{Bi} = -1.68$ eV, $\Delta\mu_I = -0.65$ eV); C ($\Delta\mu_{Ag} = -0.65$ eV, $\Delta\mu_{Bi} = -3.63$ eV, $\Delta\mu_I = 0$ eV); and D ($\Delta\mu_{Ag} = -2.06$ eV, $\Delta\mu_{Bi} = -2.22$ eV, $\Delta\mu_I = 0$ eV).

n-type electronic conductivity conversion in ABI thin films. The authors conjecture that this conversion might be correlated with point defects. Despite these experimental achievements,[7,19–22] recent reviews[15,23,24] on (Cu-Ag)-Bi-I semiconductors have emphasized the urgent need for theoretical investigation into the defect properties of ABI materials. Meanwhile, significant Ag/Bi disorder implies potential cation-exchange defect behavior, posing challenges for theoretical modeling of the ABI system.[11] It should be noted that new methods, such as machine learning[25–27] and Wyckoff position splitting,[28] have been adopted to predict the reasonable structure of ABI systems, which makes it possible to study the defect properties of these systems theoretically.

Here, using $AgBiI_4$ as an example, we perform density functional theory (DFT)[29,30] calculations to explore the electronic structure and defect properties of this material. Our results show that the dominant intrinsic defects in $AgBiI_4$ are acceptor-like V_{Ag} and Ag_{Bi}, and donor-like Ag_i and Bi_{Ag}. We reveal the nature of defects related to local structural distortion. Additionally, the calculated results suggest that synthesizing the material under I-rich conditions with a delicate ratio between Ag and Bi suppresses the formation of deep-level defects.

The detailed calculation methodology is described in the supplementary material.[25,31–39] All calculations in this work are based on the structure proposed by Barone *et al.*[25] They conducted a random forest model for DFT calculations by examining all possible 12 870 cell combinations containing 48 atoms to explore the potential positions of Ag and Bi. Their work reported the lowest energy structure for specific arrangements of Ag and Bi positions within the cell. $AgBiI_4$ with a space group of Fd3m, features Ag^+ and Bi^{3+} cations octahedrally coordinated by six iodine atoms and is described by alternating edge sharing ordered layers of $[AgI_6]^{5-}$ and $[BiI_6]^{3-}$ as shown in Fig. 1(b).[11] The lattice constants calculated with different functionals are summarized in Table I, which agree well with experimental values.[40]

We first check the dynamic and thermodynamic stability of the structure. As shown in Fig. 1(c), the 0 K phonon spectrum of the structure exhibits no imaginary frequencies throughout the Brillouin zone, confirming its dynamic stability. Thermodynamic stability requires satisfying the conditions outlined in Sec. 1 of the supplementary material. According to these constraints, the chemical potentials $\Delta\mu_{Ag}$, $\Delta\mu_{Bi}$, and $\Delta\mu_I$ that stabilize $AgBiI_4$ are bound in a polyhedron as shown in Fig. 1(d), with the phase diagram of $AgBiI_4$ based on the data from Table S3. Figure 1(d) displays a wide range of chemical potentials that can stabilize $AgBiI_4$, indicating its high thermodynamic stability.[4,11,41] We select four points in Fig. 1(d) to represent distinct $AgBiI_4$ growth conditions for subsequent defect calculations: point A (I-moderate, Ag-poor, and Bi-rich), point B (I-moderate, Ag-rich, and Bi-poor), point C (I-rich, Ag-moderate, and Bi-poor), and point D (I-rich, Ag-poor, and Bi-moderate).

The calculated bandgaps with various functionals are tabulated in Table I, and a comparison of band structures and density of states (DOS) is illustrated in Fig. S1. For clarity, we present only the band structures calculated using PBE and HSE+SOC in Figs. 2(a) and 2(c). The calculated bandgaps are 1.92 and 1.99 eV for PBE and HSE+SOC functionals. These values are consistent with both experimental (1.7–1.9 eV)[4,6,7,41] and theoretical (1.8–2.04 eV)[11,26] reports, confirming the reliability of our calculations. In comparison, PBE+SOC and HSE functional either underestimates or overestimates the bandgap of $AgBiI_4$, which will not be discussed in subsequent sections. The small bandgap difference between PBE and HSE+SOC functionals indicates significant error cancelation in PBE functionals, which is similar to that in iodine-based perovskites.[42,43] Nonetheless, the SOC effect for heavy Bi atoms is essentially important in evaluating the electronic properties. Our calculations reveal that the inclusion of SOC yields a shift of the conduction band minimum (CBM) from the R point to the Γ point, converting the indirect bandgap nature of the PBE calculation to a direct one. This can be attributed to the small direct-indirect splitting (0.07 eV) nature of the bandgap of $AgBiI_4$.[44] A similar direct-indirect splitting of 0.03 eV has been reported in the literature.[7]

The partial charge density distributions of VBM and CBM are shown in Fig. 2(b) for PBE and Fig. 2(d) for HSE+SOC. The inclusion of SOC does not introduce any change in VBM; instead, the CBM is mainly composed of Bi *p* orbitals that undergo variations. PBE results show that the VBM is composed of the antibonding states between I *p* and Ag $d_{x^2-y^2}$ with slight d_{z^2} (e_g) due to octahedral crystal-field splitting, which is also the case for the HSE+SOC calculation. The antibonding coupling between Ag 4*d* and I 5*p* pushes up the VBM, maintaining potential defect tolerance capability. The CBM composition varies depending on the calculations. PBE calculations show that the CBM comprises antibonding states between I *p* and Bi $p_x + p_y$, whereas HSE+SOC results indicate contributions from I *p* and Bi $p_x + p_y + p_z$ orbitals. The nature of *p* states makes the conduction band more dispersive, which is more favorable for electron transport than holes. Notably, the allowed *d*/*p*-*p* optical transitions[44] are likely to cause sharp absorption in $AgBiI_4$, leading to enhanced light harvesting even for thin films.

The calculated defect formation energies and transition energy levels using the PBE calculation are shown in Fig. 3. Due to the high computational cost, the PBE functional was initially employed to screen all intrinsic point defects. Defects with low formation energies were further evaluated using different functionals, as shown in Figs. S2 and S3. The results indicate that HSE+SOC yields a similar trend in formation energy for four dominant defects (Ag_i, Ag_{Bi}, Bi_{Ag}, and V_{Ag}), demonstrating the reliability of using the PBE functional for defect analysis in $AgBiI_4$.

TABLE I. Lattice constants and bandgaps of $AgBiI_4$. The superscript "in" on the bandgap values represents the indirect bandgap, while "d" represents the direct bandgap. $\Delta E_g = E_g^{direct} - E_g^{indirect}$, where E_g^{direct} stands for the minimum direct bandgap and $E_g^{indirect}$ represents the minimum indirect bandgap.

$AgBiI_4$	PBE	PBE+SOC	HSE	HSE+SOC	Exp
Lattice constant (Å)	$a = b = 12.24$ $c = 12.05$	$a = b = 12.23$ $c = 12.01$	$a = b = 12.26$ $c = 12.07$	$a = b = 12.25$ $c = 12.05$	12.22[40]
Bandgap (eV)	1.92^{in}	1.20^{d}	2.79^{in}	1.99^{d}	1.78[7] and 1.9[41]
ΔE_g(eV)	0.070	0.073	0.071	0.069	

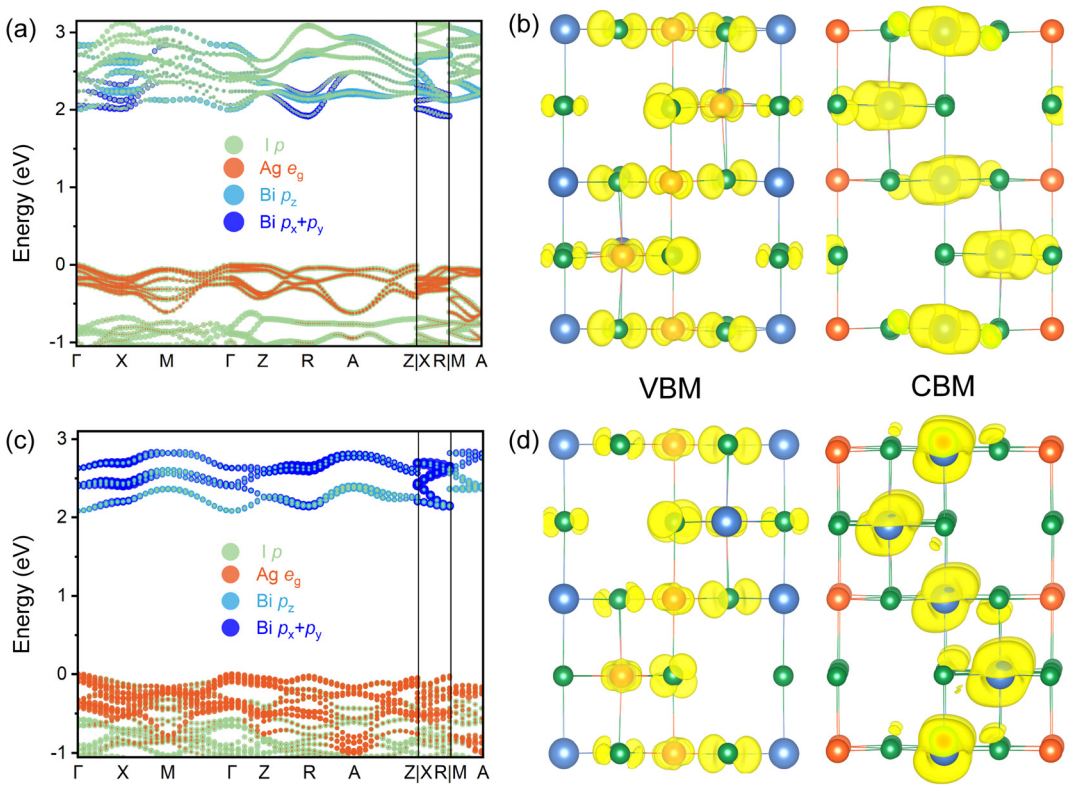

FIG. 2. Band structure of $AgBiI_4$ calculated using (a) PBE and (c) HSE+SOC. Partial charge density distribution of VBM and CBM of $AgBiI_4$ calculated using (b) PBE and (d) HSE+SOC.

Under I-moderate conditions (points A and B), the dominant defects are V_{Ag} and Bi_{Ag} at point A [Fig. 3(a)], while Ag_i and Ag_{Bi} at point B [Fig. 3(b)]. In contrast, under I-rich conditions (points C and D), the dominant defects are Ag_{Bi} at point C [Fig. 3(c)] and V_{Ag} at point D [Fig. 3(d)], respectively. At each representative chemical potential point, the Fermi level pinned by dominant defects is close to the VBM, indicating that $AgBiI_4$ should exhibit a good *p*-type conductivity, which agrees with the widely observed intrinsic *p*-type conductivity in $AgBiI_4$.[4,11,16] Among these defects, V_{Ag} is a shallow acceptor with $\varepsilon(0/1-)$ transition energy level at 2 meV above VBM. A similar shallow defect has been observed in d^{10} transition metal (Cu/Ag) vacancies within well-known photovoltaic absorbers like $CuIn_xGa_{1-x}Se_2$ (CIGS),[45] $CuZnSnS_4$ (CZTS),[46] and double perovskite $Cs_2AgBiBr_6$.[2] The formation of these Ag vacancy shallow acceptors can be attributed to the antibonding coupling between Ag 4*d* and I 5*p* orbitals, leading to a shift of the valence band maximum. Therefore, V_{Ag} is a benign defect in $AgBiI_4$ and can be considered as an efficient source for reaching favorable *p*-type conductivity. Moreover, the lattice exhibits abundant octahedral vacancies and occupied Ag 4*d*-I 5*p* antibonding states, which promote the formation of Ag vacancies. Significantly, Ag–I (virtual Ag at vacancy) and Bi–I bond lengths exhibit negligible changes upon V_{Ag} formation, as shown in Fig. 4(b). This indicates that Ag vacancy does not induce any local structural distortion; therefore, no defect states can be found within the gap as shown in Fig. 4(a). In contrast, Ag_i, as a deep donor with $\varepsilon(0/1+)$ transition level located at 0.41 eV below the CBM, is detrimental to the photovoltaic performance. Figure 4(b) shows that introducing Ag at the interstitial site will shorten the Ag–I bond length in the *xy*-plane and elongate the Bi–I bond length. Such local distortions could enhance the Ag–I interaction, leading to a reduction in the energy of Ag 5*s*-I 5*p* bonding state. Meanwhile, the elongation of the Bi–I bond length will weaken their interaction, lowering the energy of the Bi 6*p*-I 5*p* antibonding state. The combined effect of these two factors gives rise to localized defect states within the bandgap, as shown in Fig. 4(a).

Bi_{Ag} and Ag_{Bi} cation antisite defects exhibit low formation energies. Fundamentally, both Ag^+ and Bi^{3+} occupy octahedral central sites, and their ionic radii differ by only ~10% (Ag^+: 129 pm, Bi^{3+}: 117 pm). This size compatibility significantly reduces the lattice distortion energy, thereby enhancing cation migration capability. Consequently, this promotes the formation of Bi_{Ag} and Ag_{Bi} antisite defects and further intensifies the inherent cationic disorder in $AgBiI_4$.[11] Ag_{Bi} is a relatively shallow acceptor with $\varepsilon(0/1-)$ and $\varepsilon(1-/2-)$ transition levels located at 0.06 and 0.29 eV above the VBM, respectively. Substitution of Ag for Bi leads to the upward shift of Ag 4*d*-I 5*p* antibonding states. This is due to enhanced Ag–I interaction, which can be qualitatively determined by the slightly shorter Ag–I bond length [Fig. 4(b)], thus inducing an oscillated state with valence bands, as shown in Fig. 4(a). This finding is consistent with the relatively shallow nature of the charged state of the Ag_{Bi} defect. For the Bi_{Ag} antisite defect, the $\varepsilon(2+/0)$ transition energy level lies at 0.41 eV below the

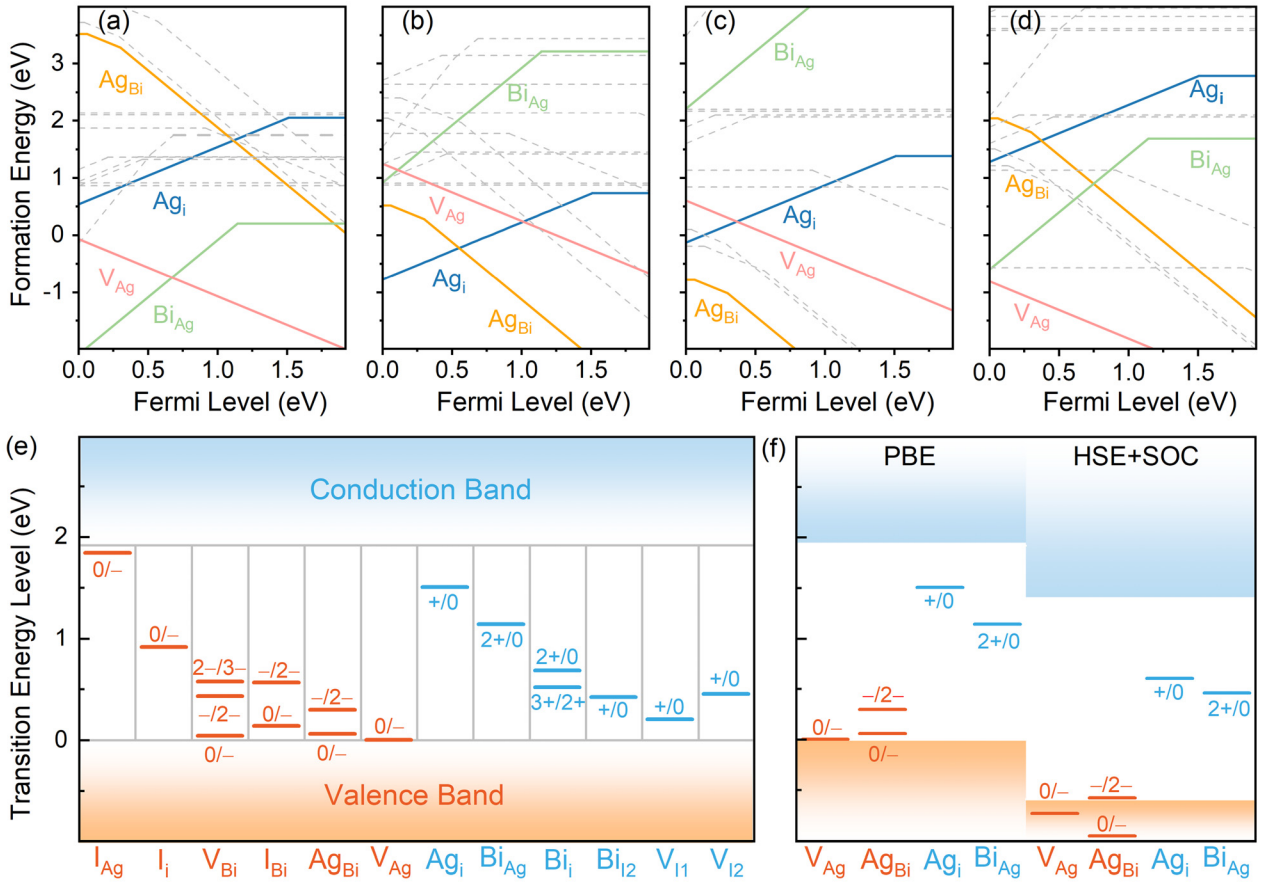

FIG. 3. Calculated formation energies of intrinsic defects in $AgBiI_4$ using PBE functional at (a) point A, (b) point B, (c) point C, and (d) point D. (e) Defect transition energy levels for $AgBiI_4$ with PBE. (f) Transition energy levels of four dominant defects with PBE and HSE+SOC.

CBM, exhibiting deep defect characteristics. Figure 4(a) shows that Bi_{Ag} also introduces a localized defect state within the bandgap, which is mainly composed of antibonding states from 6*p* orbital of the antisite Bi and 5*p* orbital of the neighboring I. Similar to the case of Ag_i, the lower energy of the antibonding states relative to the CBM originates from the weakened Bi–I interaction caused by the longer Bi–I bond length at the antisite, as shown in Fig. 4(b). It is worth noting that the calculated transition energy levels using the PBE functional are consistent with those obtained from HSE+SOC calculations, in which V_{Ag} and Ag_{Bi} retain their shallow nature, while Ag_i and Bi_{Ag} maintain their deep character. This further demonstrates the reliability of the PBE functional in analyzing the defect properties of $AgBiI_4$.

According to the earlier results, non-radiative recombination arising from deep-level defects in $AgBiI_4$ can be suppressed by optimizing the growth conditions to ensure an I-rich, Ag-poor, and Bi-moderate environment. The incorporation of hydroiodic acid (HI) into the precursor solution or the introduction of iodine vapor during the annealing process can lead an I-rich environment. Similar approaches have been successfully employed in other solar cell materials. For instance, adding sulfides to the precursor solution[47] or sulfurization using H_2S gas has proven effective in creating an S-rich environment in CZTS.[48] Similarly, incorporating I_2 into the precursor solution ensures an I-rich environment in $FAPbI_3$ [$FA{=}CH(NH_2)_2^+$] perovskites.[49] Furthermore, to ensure an Ag-poor and Bi-moderate environment, the Bi:Ag ratio should be adjusted to achieve optimal photovoltaic performance, as validated by prior studies. For instance, Wu *et al.*[13] synthesized Ag_3BiI_6 using a BiI_3:AgI molar ratio of 1:1.3, Correa Guerrero *et al.*[17] prepared Ag_2BiI_5 with a BiI_3:AgI ratio of 3:4, and Jung *et al.*[12] fabricated Ag_2BiI_5 employing a BiI_3:AgI ratio of 45:55. Although their optimal ratios varied among studies, all these studies demonstrated that incorporating an appropriate excess of BiI_3 during synthesis could effectively enhance the PCE of the solar cells. In addition, the experimental studies[10,12] have also demonstrated that the devices fabricated from the films containing a small amount of residual BiI_3 impurities exhibit enhanced performance. This observation is consistent with the findings in organic–inorganic hybrid $APbI_3$ [$A = CH(NH_2)_2^+$, $CH_3NH_3^+$] perovskite solar cells, where a small amount of residual PbI_2 impurities in the film can improve the photovoltaic efficiency through passivating surface defects and forming a type-II band offset with perovskite.[50–52] Therefore, incorporating a proper excess of BiI_3 during the synthesis of $AgBiI_4$ not only satisfies the requirements for an iodine-rich, silver-poor, and bismuth-moderate synthesis condition

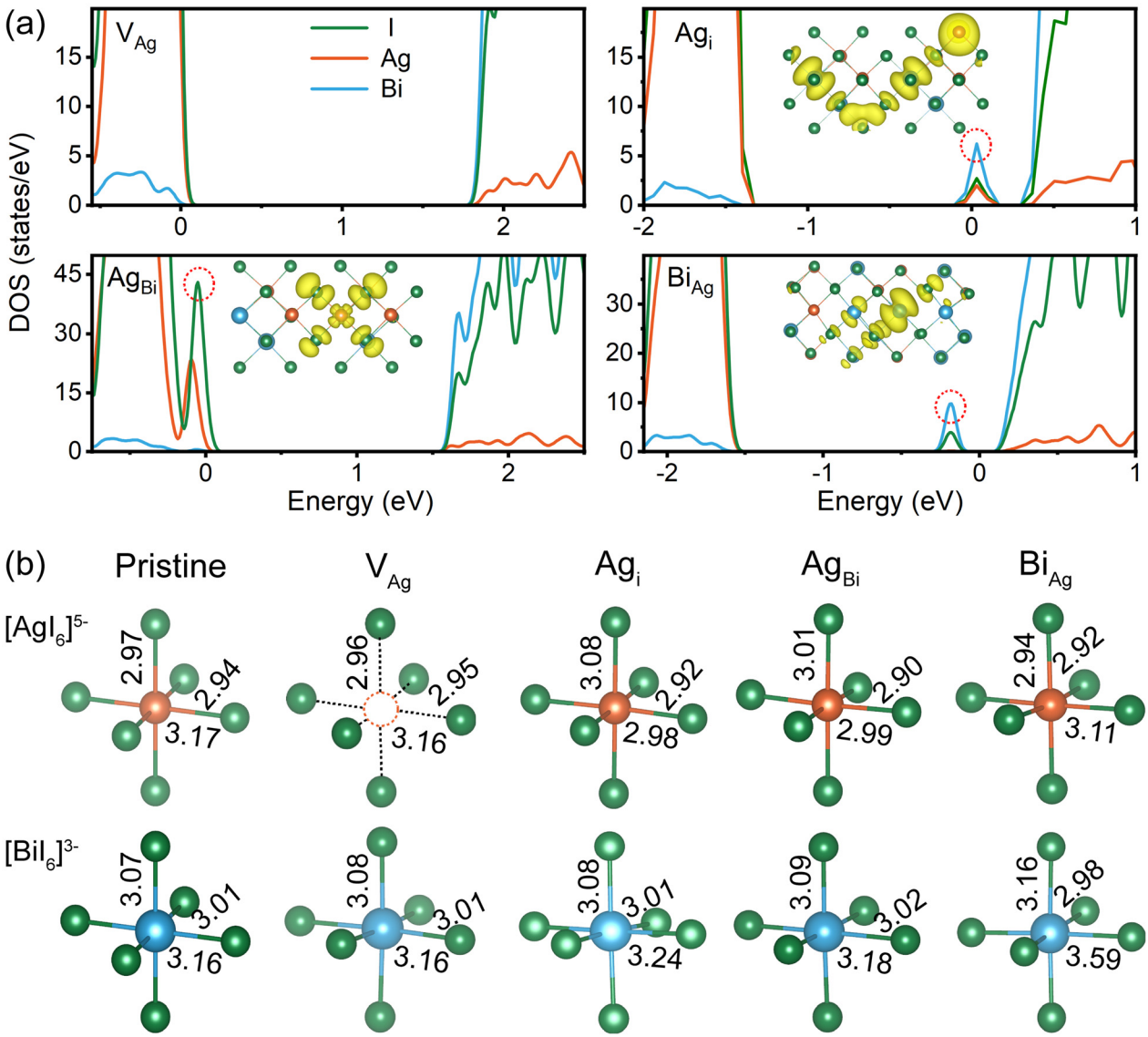

FIG. 4. (a) Density of states of the four dominant defects in the neutral charge state and partial charge density of defect states. (b) The $[AgI_6]^{5-}$ and $[BiI_6]^{3-}$ bond lengths in pristine and defective structures. The red circle with a dashed line represents a virtual atom at an Ag vacancy.

but also serves to passivate surface defects, consequently enhancing the photovoltaic performance.

In conclusion, we have systematically investigated the electronic structures and defect properties of $AgBiI_4$ using DFT calculations. Our findings reveal that $AgBiI_4$ behaves as a near-direct bandgap semiconductor, with the valence band maximum arising from Ag 4*d* and I 5*p* antibonding states, and the conduction band minimum originating from Bi 6*p* and I 5*p* states. The defect calculations show that the cation-related defects, including V_{Ag}, Ag_{Bi}, Ag_i, and Bi_{Ag}, are dominant in $AgBiI_4$. Notably, Ag_i and Bi_{Ag} exhibit deep nature, evidenced by trap states within the bandgap arising from significant structural distortion. In contrast, Ag_{Bi} and V_{Ag} defects are shallow, indicating potential defect tolerance of $AgBiI_4$. To suppress the formation of deep-level defects, we propose synthesizing the material under I-rich conditions with precise control of the Ag/Bi ratio. Additionally, strategies such as ion doping and surface passivation could be employed to further inhibit cation antisite and vacancy formation, thereby enhancing the material's structural stability and optoelectronic performance. Our detailed understanding of the defect properties is crucial for defect modulation of $AgBiI_4$, thereby enhancing its performance for photovoltaic and optoelectronic applications. These insights provide a solid foundation for future theoretical and experimental investigations into defect physics within $AgBiI_4$ and related ABI systems.

See the supplementary material for details on the computational method, band structures, defect formation energies, transition energy levels calculated with different functionals, data on V_{OC} loss, and PCE for ABI-based solar cells.

We would like to express our gratitude to the High-Performance Computing Center of Shanghai University and the Shanghai Engineering Research Center of Intelligent Computing Systems (Project No. 19DZ2252600) for providing computing resources and technical support. This work was supported by the National Natural Science Foundation of China (Grant No. 12175131).

AUTHOR DECLARATIONS

Conflict of Interest

The authors have no conflicts to disclose.

Author Contributions

Quanhe Yan: Conceptualization (equal); Data curation (equal); Writing – review & editing (equal). **Haoze Li:** Data curation (equal); Formal analysis (equal); Methodology (supporting). **Zhongyi Luo:** Methodology (supporting). **Haoyu Cao:** Methodology (supporting). **Rasha A. Awni:** Writing – review & editing (equal). **Run Xu:** Funding acquisition (equal); Methodology (supporting). **Weiwei Meng:** Formal analysis (equal); Methodology (equal); Supervision (equal); Writing – review & editing (equal). **Fei Xu:** Funding acquisition (equal); Supervision (equal); Writing – review & editing (equal). **Feng Hong:** Conceptualization (equal); Formal analysis (equal); Funding acquisition (equal); Methodology (equal); Software (equal); Supervision (equal); Writing – review & editing (equal).

DATA AVAILABILITY

The data that support the findings of this study are available from the corresponding authors upon reasonable request.

REFERENCES

[1]A. Kojima, K. Teshima, Y. Shirai, and T. Miyasaka, "Organometal halide perovskites as visible-light sensitizers for photovoltaic cells," J. Am. Chem. Soc. **131**, 6050–6051 (2009).
[2]Z. Xiao, W. Meng, J. Wang, and Y. Yan, "Thermodynamic stability and defect chemistry of bismuth-based lead-free double perovskites $Cs_2AgBiBr_6$," ChemSusChem **9**, 2628–2633 (2016).
[3]Y. Kim, Z. Yang, A. Jain, O. Voznyy, G. H. Kim, M. Liu, L. N. Quan, F. P. García de Arquer, R. Comin, J. Z. Fan *et al.*, "Pure cubic-phase hybrid iodobismuthates $AgBi_2I_7$ for thin-film photovoltaics," Angew. Chem. Int. Ed. **55**, 9586–9590 (2016).
[4]B. Ghosh, B. Wu, X. Guo, P. C. Harikesh, R. A. John, T. Baikie, Arramel, A. T. S. Wee, C. Guet, T. C. Sum *et al.*, "Superior performance of silver bismuth iodide photovoltaics fabricated via dynamic hot-casting method under ambient conditions," Adv. Energy Mater. **8**, 1802051 (2018).
[5]H. Zhu, A. Erbing, H. Wu, G. J. Man, S. Mukherjee, C. Kamal, M. B. Johansson, H. Rensmo, M. Odelius, and E. M. J. Johansson, "Tuning the bandgap in silver bismuth iodide materials by partly substituting bismuth with antimony for improved solar cell performance," ACS Appl. Energy Mater. **3**, 7372–7382 (2020).
[6]I. Turkevych, S. Kazaoui, E. Ito, T. Urano, H. Tomiyasu, H. Yamagishi, M. Kondo, K. Yamada, and S. Aramaki, "Photovoltaic rudorffites: Lead-free silver bismuth halides alternative to hybrid lead halide perovskites," Energy Technol. **10**, 3754–3759 (2017).
[7]H. Zhu, M. Pan, M. B. Johansson, and E. M. J. Johansson, "High photon-to-current conversion in solar cells based on light-absorbing silver bismuth iodide," ChemSusChem **10**, 2592–2596 (2017).
[8]Z. Shao, T. Le Mercier, M. B. Madec, and T. Pauporté, "Exploring $AgBi_xI_{3x+1}$ semiconductor thin films for lead-free perovskite solar cells," Mater. Des. **141**, 81–87 (2018).
[9]N. Pai, J. Lu, T. R. Gengenbach, A. Seeber, A. S. R. Chesman, L. Jiang, D. C. Senevirathna, P. C. Andrews, U. Bach, Y. B. Cheng *et al.*, "Silver bismuth sulfoiodide solar cells: Tuning optoelectronic properties by sulfide modification for enhanced photovoltaic performance," Adv. Energy Mater. **9**, 1803396 (2019).
[10]A. Kulkarni, A. K. Jena, M. Ikegami, and T. Miyasaka, "Performance enhancement of $AgBi_2I_7$ solar cells by modulating a solvent-mediated adduct and tuning remnant BiI_3 in one-step crystallization," Chem. Commun. **55**, 4031–4034 (2019).
[11]H. C. Sansom, G. F. S. Whitehead, M. S. Dyer, M. Zanella, T. D. Manning, M. J. Pitcher, T. J. Whittles, V. R. Dhanak, J. Alaria, J. B. Claridge *et al.*, "$AgBiI_4$ as a lead-free solar absorber with potential application in photovoltaics," Chem. Mater. **29**, 1538–1549 (2017).
[12]K. W. Jung, M. R. Sohn, H. M. Lee, I. S. Yang, S. D. Sung, J. Kim, E. Wei-Guang Diau, and W. I. Lee, "Silver bismuth iodides in various compositions as potential Pb-free light absorbers for hybrid solar cells," Sustainable Energy Fuels **2**, 294–302 (2018).
[13]M.-C. Wu, Q.-H. Wang, K.-C. Hsiao, S.-H. Chen, C.-M. Ho, M.-H. Jao, Y.-H. Chang, and W.-F. Su, "Composition engineering to enhance the photovoltaic performance and to prolong the lifetime for silver bismuth iodide solar cell," Chem. Eng. J. Adv. **10**, 100275 (2022).
[14]Y. Peng, T. N. Huq, J. Mei, L. Portilla, R. A. Jagt, L. G. Occhipinti, J. L. MacManus-Driscoll, R. L. Z. Hoye, and V. Pecunia, "Lead-free perovskite-inspired absorbers for indoor photovoltaics," Adv. Energy Mater. **11**, 2002761 (2020).
[15]G. K. Grandhi, D. Hardy, M. Krishnaiah, B. Vargas, B. Al-Anesi, M. P. Suryawanshi, D. Solis-Ibarra, F. Gao, R. L. Z. Hoye, and P. Vivo, "Wide-bandgap perovskite-inspired materials: Defect-driven challenges for high-performance optoelectronics," Adv. Funct. Mater. **34**, 2307441 (2024).
[16]M. Khazaee, K. Sardashti, C.-C. Chung, J.-P. Sun, H. Zhou, E. Bergmann, W. A. Dunlap-Shohl, Q. Han, I. G. Hill, J. L. Jones *et al.*, "Dual-source evaporation of silver bismuth iodide films for planar junction solar cells," J. Mater. Chem. A **7**, 2095–2105 (2019).
[17]N. B. Correa Guerrero, Z. Guo, N. Shibayama, A. K. Jena, and T. Miyasaka, "A semitransparent silver-bismuth iodide solar cell with V_{oc} above 0.8 V for indoor photovoltaics," ACS Appl. Energy Mater. **6**, 10274–10284 (2023).
[18]A. Merker, M. Morgenroth, M. Scholz, T. Lenzer, and K. Oum, "Critical evaluation of the photovoltaic performance of $(AgI)_x$ $(BiI_3)_y$ thin films from the viewpoint of ultrafast spectroscopy and photocurrent experiments," J. Phys. Chem. C **127**, 1487–1498 (2023).
[19]V. Pecunia, J. Zhao, C. Kim, B. R. Tuttle, J. Mei, F. Li, Y. Peng, T. N. Huq, R. L. Z. Hoye, N. D. Kelly *et al.*, "Assessing the impact of defects on lead-free perovskite-inspired photovoltaics via photoinduced current transient spectroscopy," Adv. Energy Mater. **11**, 2003968 (2021).
[20]A. Bera, S. Paramanik, A. Maiti, and A. J. Pal, "Energy landscape in silver-bismuth-iodide rudorffites: Combining scanning tunneling spectroscopy and Kelvin probe force microscopy," Phys. Rev. Mater. **5**, 095404 (2021).
[21]A. Matuhina, G. K. Grandhi, A. Bergonzoni, L. Pedesseau, R. Grisorio, S. Annurakshita, H. Ali-Löytty, R. Varghese, K. Lahtonen, G. Volonakis *et al.*, "Surface and optical properties of phase-pure silver iodobismuthate nanosrystals," Nanoscale **15**, 14764–14773 (2023).
[22]H. Wu, H. Zhu, A. Erbing, M. B. Johansson, S. Mukherjee, G. J. Man, H. Rensmo, M. Odelius, and E. M. J. Johansson, "Bandgap tuning of silver bismuth iodide via controllable bromide substitution for improved photovoltaic performance," ACS Appl. Energy Mater. **2**, 5356–5362 (2019).
[23]A. Chakraborty, N. Pai, J. Zhao, B. R. Tuttle, A. N. Simonov, and V. Pecunia, "Rudorffites and beyond: Perovskite-inspired silver/copper pnictohalides for next-generation environmentally friendly photovoltaics and optoelectronics," Adv. Funct. Mater. **32**, 2203300 (2022).

[24]H. Zhu, I. Turkevych, H. Lohan, P. Liu, R. W. Martin, F. C. P. Massabuau, and R. L. Z. Hoye, "Progress and applications of (Cu-)Ag-Bi-I semiconductors, and their derivatives, as next-generation lead-free materials for photovoltaics, detectors and memristors," Int. Mater. Rev. **69**, 19–62 (2024).
[25]V. T. Barone, B. R. Tuttle, and S. V. Khare, "Properties of $AgBiI_4$ using high throughput DFT and machine Learning methods," J. Appl. Phys. **131**, 245701 (2022).
[26]V. T. Barone, B. R. Tuttle, and S. V. Khare, "Spherical cluster method for ground state determination of site-disordered materials: Application to $Ag_xBi_yI_{x+3y}$," Comput. Mater. Sci. **231**, 112587 (2024).
[27]C. S. Khare, V. T. Barone, and R. E. Irving, "Investigation of optoelectronic properties of $AgSbI_4$ using machine learning and first principles methods," J. Phys. Chem. Solids **187**, 111803 (2024).
[28]B. Cucco, L. Pedesseau, C. Katan, J. Even, M. Kepenekian, and G. Volonakis, "Silver-bismuth halide double salts for lead-free photovoltaics: Insights from symmetry-based modeling," Sol. RRL **6**, 2200718 (2022).
[29]P. Hohenberg and W. Kohn, "Inhomogeneous electron gas," Phys. Rev. **136**, B864–B871 (1964).
[30]W. Kohn and L. J. Sham, "Self-consistent equations including exchange and correlation effects," Phys. Rev. **140**, A1133–A1138 (1965).
[31]G. Kresse and J. Hafner, "*Ab initio* molecular dynamics for liquid metals," Phys. Rev. B **47**, 558–561 (1993).
[32]G. Kresse and J. Hafner, "*Ab initio* molecular-dynamics simulation of the liquid-metal-amorphous-semiconductor transition in germanium," Phys. Rev. B **49**, 14251–14269 (1994).
[33]J. P. Perdew, K. Burke, and M. Ernzerhof, "Generalized gradient approximation made simple," Phys. Rev. Lett. **77**, 3865 (1996).
[34]J. Heyd, G. E. Scuseria, and M. Ernzerhof, "Erratum: 'Hybrid functionals based on a screened Coulomb potential' [J. Chem. Phys. **118**, 8207 (2003)]," J. Chem. Phys. **124**, 219906 (2006).
[35]V. Wang, N. Xu, J.-C. Liu, G. Tang, and W.-T. Geng, "VASPKIT: A user-friendly interface facilitating high-throughput computing and analysis using VASP code," Comput. Phys. Commun. **267**, 108033 (2021).
[36]K. Momma and F. Izumi, "VESTA 3 for three-dimensional visualization of crystal, volumetric and morphology data," J. Appl. Crystallogr. **44**, 1272–1276 (2011).
[37]A. Togo and I. Tanaka, "First principles phonon calculations in materials science," Scr. Mater. **108**, 1–5 (2015).
[38]S.-H. Wei, "Overcoming the doping bottleneck in semiconductors," Comput. Mater. Sci. **30**, 337–348 (2004).
[39]M. Chagas da Silva, M. Lorke, B. Aradi, M. Farzalipour Tabriz, T. Frauenheim, A. Rubio, D. Rocca, and P. Deák, "Self-consistent potential correction for charged periodic systems," Phys. Rev. Lett. **126**, 076401 (2021).
[40]T. Oldag, T. Aussieker, H. L. Keller, C. Preitschaft, and A. Pfitzner, "Solvothermale synthese und bestimmung der kristallstrukturen von $AgBiI_4$ und Ag_3BiI_6," Z. Anorg. Allg. Chem. **631**, 677–682 (2005).
[41]C. Lu, J. Zhang, H. Sun, D. Hou, X. Gan, M-h Shang, Y. Li, Z. Hu, Y. Zhu, and L. Han, "Inorganic and lead-free $AgBiI_4$ rudorffite for stable solar cell applications," ACS Appl. Energy Mater. **1**, 4485–4492 (2018).
[42]R. Jono and H. Segawa, "Theoretical study of the band-gap differences among lead triiodide perovskite materials: $CsPbI_3$, $MAPbI_3$, and $FAPbI_3$," Chem. Lett. **48**, 877–880 (2019).
[43]J.-J. Yang, W.-K. Chen, X.-Y. Liu, W.-H. Fang, and G. Cui, "Spin-orbit coupling is the key to promote asynchronous photoinduced charge transfer of two-dimensional perovskites," JACS Au **1**, 1178–1186 (2021).
[44]S. Nair, V. Kashid, A. Punde, S. Shah, A. Waghmare, Y. Hase, P. Shinde, B. Bade, V. Doiphode, S. Ladhane *et al.*, "A combined theoretical and experimental investigation of 3D ternary perovskite-like silver iodobismuthate," ChemistrySelect **8**, e202301582 (2023).
[45]A. Miglio, C. P. Heinrich, W. Tremel, G. Hautier, and W. G. Zeier, "Local bonding influence on the band edge and band gap formation in quaternary chalcopyrites," Adv. Sci. **4**, 1700080 (2017).
[46]S. Chen, A. Walsh, X. G. Gong, and S. H. Wei, "Classification of lattice defects in the kesterite Cu_2ZnSnS_4 and $Cu_2ZnSnSe_4$ earth-abundant solar cell absorbers," Adv. Mater. **25**, 1522–1539 (2013).
[47]M. Johnson, S. V. Baryshev, E. Thimsen, M. Manno, X. Zhang, I. V. Veryovkin, C. Leighton, and E. S. Aydil, "Alkali-metal-enhanced grain growth in Cu_2ZnSnS_4 thin films," Energy Environ. Sci. **7**, 1931–1938 (2014).
[48]I. Akyuz, F. Atay, R. Aydin, and S. Kose, "Production and characterization of CZTS films: On the role of H_2S flow rate," Sol. Energy **194**, 709–715 (2019).
[49]Y. Zhang, Y. Chen, G. Liu, Y. Wu, Z. Guo, R. Fan, K. Li, H. Liu, Y. Zhao, and T. J. S. Kodalle, "Nonalloyed α-phase formamidinium lead triiodide solar cells through iodine intercalation," Science **387**, 284–290 (2025).
[50]Q. Jiang, Z. Chu, P. Wang, X. Yang, H. Liu, Y. Wang, Z. Yin, J. Wu, X. Zhang, and J. You, "Planar-structure perovskite solar cells with efficiency beyond 21%," Adv. Mater. **29**, 1703852 (2017).
[51]W.-S. Tseng, M.-H. Jao, C.-C. Hsu, J.-S. Huang, C.-I. Wu, and N. C. Yeh, "Stabilization of hybrid perovskite $CH_3NH_3PbI_3$ thin films by graphene passivation," Nanoscale **9**, 19227–19235 (2017).
[52]J. Un-GI, C.-J. Yu, Y.-H. Kye, Y.-S. Kim, C.-H. Kim, and S.-G. Ri, "A first-principles study on the chemical stability of inorganic perovskite solid solutions $Cs_{1-x}Rb_xPbI_3$ at finite temperature and pressure," J. Mater. Chem. A **6**, 17994–18002 (2018).